

Proximity-induced Josephson π -Junctions in Topological Insulators

Constantin Schrader, A. A. Zyuzin, Jelena Klinovaja, and Daniel Loss

Department of Physics, University of Basel, Klingelbergstrasse 82, CH-4056 Basel, Switzerland

(Dated: July 1, 2015)

We study two microscopic models of topological insulators in contact with an s -wave superconductor. In the first model the superconductor and the topological insulator are tunnel coupled via a layer of scalar and of randomly oriented spin impurities. Here, we require that spin-flip tunneling dominates over spin-conserving one. In the second model the tunnel coupling is realized by an array of single-level quantum dots with randomly oriented spins. It is shown that the tunnel region forms a π -junction where the effective order parameter changes sign. Interestingly, due to the random spin orientation the effective descriptions of both models exhibit time-reversal symmetry. We then discuss how the proposed π -junctions support topological superconductivity without magnetic fields and can be used to generate and manipulate Kramers pairs of Majorana fermions by gates.

PACS numbers: 74.50.+r, 71.10.Pm, 74.45.+c

Introduction. When two s -wave superconductors (SCs) are brought into contact via an insulator the energy of the system in equilibrium is minimized when the relative phase between the two superconducting order parameters vanishes. Interestingly, when the insulator is doped with magnetic impurities, it was shown by theory [1] and experiment [2] that spin-flip tunneling can induce an equilibrium ground state with a relative phase difference of π between the superconducting order parameters, building up a so-called Josephson π -junction ($J\pi J$). It was predicted [3] and experimentally confirmed [4] that a $J\pi J$ can be generated by replacing the layer of magnetic impurities by a ferromagnetic metal. A $J\pi J$ can also arise when two SCs are tunnel-coupled through an intermediate resonant state in the presence of strong Coulomb interactions [5], as observed in a system of two SCs coupled by a quantum dot (QD) occupied by a single electron [6]. In recent experiments [7–9] it was demonstrated that superconductivity can also be proximity-induced in the helical edge states of a topological insulator (TI) material [10–18] via coupling to an external s -wave SC. These experimental advances have also stimulated the theoretical interest in Josephson junctions based on TIs [19–21]. Motivated by the existence of ordinary $J\pi Js$ an important and immediate question is: Are there microscopic mechanisms allowing one to induce a superconducting order parameter in the helical edge states of the TI that is of *opposite* relative sign compared to the one of the external s -wave SC, ideally without breaking time-reversal invariance (TRI)? In this work we answer this question in the affirmative.

We propose two setups involving TIs in which such a π -junction is shown to emerge. In the first setup the tunnel coupling is realized by a thin insulating layer of scalar and magnetic impurities with randomly oriented spins. Here we require that spin-flip tunneling dominates over normal tunneling. In the second setup the tunnel coupling is realized by an array of single-level QDs, each of which is occupied by a single spin with random orienta-

tion. Critically, the random orientation of spins preserves TRI in an effective description. We note that both setups can be realized by combining the already existing experiments on proximity-inducing superconductivity solely in the edge states of a TI [7–9] and the experiments on $J\pi Js$ in SC-magnetic insulator-SC [2] and SC-QD-SC devices [6]. We note that the same setup could be assembled in the framework of strip of stripes models [22–28] based on an array of coupled one-dimensional channels with spin-orbit interaction [27]. As a striking consequence we find that the proposed models for proximity-induced $J\pi Js$ in a TI provide an alternative approach to engineer Kramers pairs of Majorana fermions (MFs) [29–39] easily movable by gates. Remarkably, no magnetic fields are needed. More precisely we consider two TI samples that form a proximity-induced $J\pi Js$ with respect to one another and allow for tunneling between them in the finite space region, at the ends of which the MFs emerge.

Josephson junction models. In the first model we consider a bulk s -wave SC connected by a tunnel contact to the edge of a 2D TI, see Fig. 1(a). The Hamiltonian of the system is given by

$$H_1 = H_{\text{BCS}} + H_{\text{TI}} \quad (1)$$

$$+ \frac{1}{2} \int d\mathbf{r} dx [\Psi^\dagger(\mathbf{r}) \cdot \bar{T}_1(\mathbf{r}, x) \Phi(x) + \text{H.c.}],$$

with the tunneling matrix $\bar{T}_1(\mathbf{r}, x) = T_1(\mathbf{r}, x)(1 + \tau^z)/2 - T_1^*(\mathbf{r}, x)(1 - \tau^z)/2$. Here, $H_{\text{BCS}} = (1/2) \int d\mathbf{r} \Psi^\dagger(\mathbf{r}) \cdot [-(\hbar^2 \partial_{\mathbf{r}}^2 / 2m + \mu) \tau^z - \Delta_{sc} \sigma^y \tau^y] \Psi(\mathbf{r}) + \text{H.c.}$ is the BCS Hamiltonian of the SC, μ being the chemical potential in the SC and m being the electron mass, and $H_{\text{TI}} = (1/2) \int dx [\Phi^\dagger(x) \cdot (-i\hbar v_F \sigma^z \partial_x) \Phi(x) + \text{H.c.}]$ is the Hamiltonian of the TI edge with the Fermi velocity v_F . Without loss of generality, we assume that the superconducting order parameter Δ_{sc} is positive. The electron Nambu operator in the SC (TI) is given by $\Psi(\mathbf{r}) = (\Psi_\uparrow(\mathbf{r}), \Psi_\downarrow(\mathbf{r}), \Psi_\uparrow^\dagger(\mathbf{r}), \Psi_\downarrow^\dagger(\mathbf{r}))$ [$\Phi(x) = (R(x), L(x), R^\dagger(x), L^\dagger(x))$]. The Pauli matrices τ^a (σ^a)

with $a = x, y, z$ act in particle-hole (spin) space. The slowly-varying spin-up (spin-down) right (left) mover fields $R(x)$ [$L(x)$] are defined around the Fermi points $\pm k_F$ which in turn are determined by the position of the chemical potential μ_{TI} in the TI defined with respect to the Dirac point. The last term in Eq. (1) describes the tunneling between points \mathbf{r} of the SC and points x on the edge of the TI. The interface between the SC and the TI is assumed to be rough, which means that the thinnest regions of the interface give the highest probability for electrons to tunnel between the SC and the TI. We model these thinnest regions located at points x_ℓ by point contacts. The tunnel contact between the SC and the TI is doped with scalar and magnetic impurities with randomly oriented spins $\mathbf{S}_{\ell,k} = (S_{\ell,k}^x, S_{\ell,k}^y, S_{\ell,k}^z)$. Here $\mathbf{S}_{\ell,k}$ is the operator of the k -th localized spin close to the point contact x_ℓ on the TI sample. The tunneling occurs via the virtual states of the scalar and magnetic impurities. The tunneling matrix amplitude is given by

$$T_1(\mathbf{r}, x) = \delta(\mathbf{r} - x \mathbf{e}_x) \quad (2)$$

$$\times \sum_{\ell,k} \delta(x - x_\ell) \left[t_k + \sum_{a=x,y,z} u_k^a \sigma^a S_{\ell,k}^a \right].$$

Here, \mathbf{e}_x is a unit vector pointing along the TI edge written in terms of the coordinates of the SC. The normal (spin-flip) tunneling is parametrized by a complex amplitude t_k (u_k^a) with scalar impurities contributing to the amplitude t_k only. This model implies that there can be more than one magnetic or scalar impurity at the vicinity of the point contact.

In the second model we consider the coupling of a bulk s -wave SC to a 2D TI via an array of single-level QDs, see Fig. 1(b). The Hamiltonian of the system is given by

$$H_2 = H_{\text{BCS}} + H_{\text{TI}} + H_{\text{D}} \quad (3)$$

$$+ \frac{1}{2} \sum_j \left[t_{j,1} D_j^\dagger \cdot \tau^z \Psi(\mathbf{r}_j) + t_{j,2} D_j^\dagger \cdot \tau^z \Phi(x_j) + \text{H.c.} \right].$$

Here, $H_{\text{D}} = (1/2) \sum_j (-\epsilon_j D_j^\dagger \cdot \tau^z D_j + U_j n_{j,\uparrow} n_{j,\downarrow}) + \text{H.c.}$ is the Hamiltonian of an array of single-level QDs at energies $\epsilon_j > 0$ and with amplitudes U_j of the Coulomb interaction on the QDs and $D_j = (D_{j,\uparrow}, D_{j,\downarrow}, D_{j,\uparrow}^\dagger, D_{j,\downarrow}^\dagger)$ is the electron Nambu operator on the j th QD. The occupation number operators for spin-up and spin-down electrons on the j th QD are given by $n_{j,\uparrow} = D_{j,\uparrow}^\dagger D_{j,\uparrow}$ and $n_{j,\downarrow} = D_{j,\downarrow}^\dagger D_{j,\downarrow}$. Tunneling occurs at points \mathbf{r}_j and x_j on the SC and the TI, respectively, and is described by tunneling amplitudes $t_{j,1}$ and $t_{j,2}$.

Proximity-induced $J\pi$ Js. We first discuss the model shown in Fig. 1(a) and described by Eqs. (1) and (2). We neglect the inverse proximity effect due to magnetic impurities. By integrating out the degrees of freedom of the SC and including contributions up to second order in the tunneling amplitudes we see that the equation

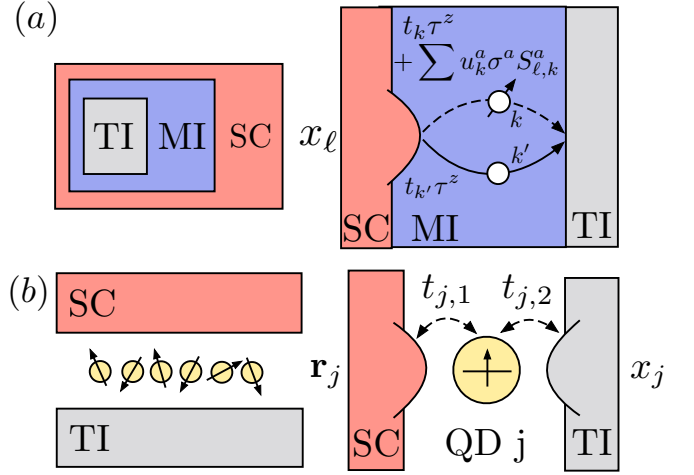


FIG. 1: (Color online) Setups to generate a proximity-induced Josephson π -junction in topological insulators (TIs). a) An s -wave SC (red) couples to a TI (grey) via an insulator doped with magnetic and scalar impurities (MI, magnetic insulator, blue). If the spin-flip tunneling rates are larger than the normal tunneling rates superconducting gaps with opposite sign are induced in the TI samples. b) Instead of the MI the SC is coupled to the TI via an array of single-level QDs in the Coulomb blockade regime. The array of QDs is occupied with randomly oriented electron spins.

of motion for the Green's function $g(x, x')$ of the TI in frequency space is given by

$$g^{-1}(x) \cdot g(x, x') = \delta(x - x') + \int dx_1 \Sigma(x, x_1) \cdot g(x_1, x') \quad (4)$$

with $g^{-1}(x) = i\omega + i\hbar v_F \sigma^z \partial_x$ and ω the fermionic Matsubara frequency. In leading order, the electron self-energy in the TI is given by

$$\Sigma(x, x_1) = \int d^3r d^3r' T_1^\dagger(\mathbf{r}, x) \cdot G(\mathbf{r} - \mathbf{r}') \cdot T_1(\mathbf{r}', x_1). \quad (5)$$

Here, $G(\mathbf{r} - \mathbf{r}')$ denotes the Green's function of the bare clean homogeneous three-dimensional SC defined by $G^{-1}(\mathbf{r}) \cdot G(\mathbf{r} - \mathbf{r}') = \delta(\mathbf{r} - \mathbf{r}')$ with $G^{-1}(\mathbf{r}) = i\omega + (\hbar^2 \partial_{\mathbf{r}}^2 / 2m + \mu) \tau^z - \Delta_{sc} \sigma^y \tau^y$. At vanishing relative distance a solution to this equation is given

$$G(\mathbf{r} = 0) = \frac{-\pi\nu}{\sqrt{\omega^2 + \Delta_{sc}^2}} [\Delta_{sc} \sigma^y \tau^y + i\omega], \quad (6)$$

with $\nu = \frac{m p_F}{2\pi^2}$ the normal-state density of states per spin and p_F the Fermi momentum in the SC. We adopt several assumptions to simplify Eq. (5). First, the distribution of impurities is assumed to be almost continuous and hence sums over impurities at discrete positions are replaced by integrals over impurity densities. Second, terms that are linear in the Pauli matrices σ^a vanish after averaging over the random orientation of the spins $\mathbf{S}_{\ell,k}$. Third, at some fixed x_ℓ tunneling contributions from points $x_{\ell'}$ for

$\ell' \neq \ell$ can be neglected. The contribution of these terms to the effective Hamiltonian can be incorporated in the chemical potential [40]. These assumptions imply that

$$\int dx_1 \Sigma(x, x_1) \cdot g(x_1, x') \approx - \left[i\omega(\Gamma + \Gamma_S) - \Delta_{sc}(\Gamma - \Gamma_S)\sigma^y\tau^y \right] \cdot \frac{g(x, x')}{\sqrt{\omega^2 + \Delta_{sc}^2}}, \quad (7)$$

with the scattering rates

$$\Gamma = \pi\nu n_0 \left| \sum_k t_k \right|^2, \quad (8)$$

$$\Gamma_S = \pi\nu n_S S(S+1) \sum_{k,a} |u_k^a|^2 / 3. \quad (9)$$

Here, n_0 is the concentration of point contacts that allow for spin-conserved tunneling, while n_S is the concentration of point contacts that allow for spin-flip tunneling. We note that $\langle \mathbf{S}_{\ell,k} \mathbf{S}_{\ell',k'} \rangle = S(S+1)\delta_{\ell\ell'}\delta_{kk'}$, with $\langle \dots \rangle$ meaning the average over random spin directions and S being the magnitude of the impurity spin. In particular, the average vanishes for different impurity spins. This implies that in the expression for the scattering rate Γ_S terms $\propto u_k^a u_{k'}^a$, with $k \neq k'$ vanish as well. The effective order parameter in the TI for $\omega \ll \Delta_{sc}, \Gamma, \Gamma_S$ is given by

$$\Delta_{\Gamma, \Gamma_S} \approx \Gamma - \Gamma_S. \quad (10)$$

Interestingly, if $\Gamma_S > \Gamma$ the effective order parameter can become negative. Such a situation naturally emerges if the tunnel contact contains a large number of magnetic and scalar impurities. At a particular point x_ℓ the electron tunneling amplitude via some magnetic impurity k is $t_k + \sum_a u_k^a \sigma^a S_{\ell,k}^a$ and $t_{k'}$ for some scalar impurity k' . We assume that $|t_k| \approx |t_{k'}|$, while generally their relative sign is random. Thus, for many impurities the normal tunneling contributions in Eq. (8) destructively interfere, so that $\sum_k t_k \approx 0$. As a result, $\Gamma_S > \Gamma$ can be realized and $\Delta_{\Gamma, \Gamma_S}$ becomes negative.

Next we discuss the model of an s -wave SC coupled to a 2D TI via an array of QDs, as depicted in Fig. 1(b) and described by Eq. (3). We will work in the Coulomb blockade regime. Thus, we assume singly occupied QDs with the electron spin on the QDs being randomly oriented. In the limit of small tunneling amplitudes that couple the SC and the TI to the QD we use a Schrieffer-Wolff transformation [41] to map the Hamiltonian H_2 as given in Eq. (3) onto a Hamiltonian H_1 of the form as given in Eq. (1) with $t_k \equiv 0$. The physical interpretation is that due to the large Coulomb interactions on the QDs only spin-flip tunneling of electrons through the dots is allowed [5]. From the discussion of the first model we can conclude again that $\Gamma_S > 0$, while $\Gamma \approx 0$.

Thus, we see that in both models we obtain a $J\pi J$ in the tunneling region, *i.e.*, the proximity-induced effective superconducting order parameter in the helical edge

states of the TI assumes the opposite sign compared to the one of the SC.

Kramers pairs of Majorana fermions. In a TI proximity-coupled to an s -wave SC magnetic perturbations can be used to induce MFs [42]. However, in realistic scenarios the use of magnetic fields should be avoided since it acts detrimental on superconductivity and it is indeed not a necessary ingredient: In the absence of it Kramers pairs of MFs can emerge in nanowire systems that are coupled to unconventional SCs [29–33]. Also setups using conventional SCs in proximity to nanowires [34–37] and in 2D [38] and to 3D TIs [39] were proposed. In particular, it was predicted that Kramers pairs of MFs appear due to $J\pi J$ s in nanowires [33–35] or in 3D TI films [39]. In this section we make use of the $J\pi J$ models introduced above and propose two setups (labeled by $N = 1, 2$) that host Kramers pairs of MFs based on two 2D TIs. As a major advantage both setups are accessible by current experimental techniques in TIs [7–9] and in $J\pi J$ s based on magnetic insulators [2] and QDs [6]. Also, to reveal the non-abelian statistics the pairs can easily be moved by tuning a tunnel barrier between the TIs.

We consider two TIs labeled by $n = 1, 2$. In the first (second) setup, edge states are of opposite (same) helicity and the chemical potentials are tuned to be opposite (to be the same) with $\mu_1 = -\mu_2$ ($\mu_1 = \mu_2$), as illustrated in Fig. 2b (Fig. 2c). Both TIs are brought into proximity to an s -wave SC. In the the first TI, the tunnel contact is doped with scalar and magnetic impurities with randomly oriented spins or, equivalently, an array of QDs with randomly oriented spins is used. As shown above, a π -junction emerges and the proximity gap in the first TI acquires the opposite sign to the bulk SC, $-\Delta_1 < 0$. The tunnel contact between the SC and the second TI does not contain a spin-flip source. Thus, the corresponding order parameter is of the same sign as in the SC, $\Delta_2 > 0$. The induced superconductivity in the n th TI of the N th setup is described by the Hamiltonian

$$H_{sc,n}^{(N)} = (-1)^{(N-1)(n-1)} \frac{\Delta_n}{2} \int dx \left[L_n^\dagger R_n^\dagger - R_n^\dagger L_n^\dagger + \text{H.c.} \right] \quad (11)$$

in the basis $\Phi_n(x) = (R_n(x), L_n(x), R_n^\dagger(x), L_n^\dagger(x))$. For the first (second) TI of the first setup we have introduced slowly-varying spin-up (spin-down) right-mover $R_1(x)$ [$R_2(x)$] and spin-down (spin-up) left-mover $L_1(x)$ [$L_2(x)$] fields defined around the Fermi points $\pm k_F$. In the second setup $R_2(x)$ [$L_2(x)$] is the spin up (spin down) mode, see Fig. 2.

The two TIs are coupled via a tunnel barrier placed in the region $0 \leq x \leq L$ as shown in Fig. 2(a) Neglecting the fast-oscillating terms [43], we find that the tunneling

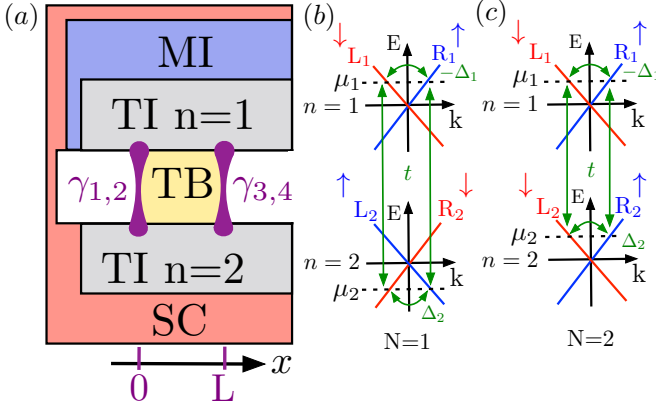


FIG. 2: (Color online) (a) Setup hosting Kramers pairs of MFs. Two TIs (grey rectangles) are placed on top of an underlying s -wave SC (red) such that proximity superconductivity is induced in both TIs. Importantly, the first TI is coupled through a magnetic insulator (MI, blue) resulting in the $J\pi J$. The tunnel barrier (TB, yellow) between the edges of two TIs extends from $x = 0$ to $x = L$. One Kramers pair of MFs $\gamma_{1,2}$ [$\gamma_{3,4}$] (purple) is localized at the $x = 0$ [$x = L$] end of the TB and can be manipulated by tuning the length L of the TB. The spectrum of two pairs of TI edge modes is considered in (b) for the first setup and in (c) for the second setup. (b) Edge modes of the same TI are coupled by proximity-induced pairing amplitudes $\Delta_1 < 0$ and $\Delta_2 > 0$, *resp.* The chemical potentials are opposite for the two TIs, $\mu_1 = -\mu_2$. The helicities of the edge states are opposite (indicated by the coloring in red and blue). The tunneling (t) couples a right-moving state in the first TI to a left-moving state in the second TI, and vice versa. (c) The two TIs have the same chemical potential, $\mu_1 = \mu_2$, and the same helicities. The tunneling (t) couples a right-[left-] moving state in the first TI to a right-[left-] moving state in the second TI.

Hamiltonian in the first setup is given by

$$H_t^{(1)} = \frac{t}{2} \int_0^L dx [e^{i\phi} (R_2^\dagger L_1 - L_1 R_2^\dagger) + e^{-i\phi} (L_2^\dagger R_1 - R_1 L_2^\dagger) + \text{H.c.}], \quad (12)$$

while in the second setup by

$$H_t^{(2)} = \frac{t}{2} \int_0^L dx [e^{i\phi} (R_2^\dagger R_1 - R_1 R_2^\dagger) + e^{-i\phi} (L_2^\dagger L_1 - L_1 L_2^\dagger) + \text{H.c.}]. \quad (13)$$

Here, t (ϕ) is the tunneling amplitude (phase) between two TIs. The choice of ϕ ensures TRI. The total Hamiltonian is $H^{(N)} = \sum_n (H_{TI,n} + H_{sc,n}^{(N)}) + H_t^{(N)}$, where the kinetic part $H_{TI,n} \equiv H_{TI}$ is identical for both TIs and was introduced in Eq. (1). The tunneling phase can be removed from the total Hamiltonian by a suitable gauge transformation [44]. In both setups, we find that a topological phase transition accompanied by the bulk gap closing and reopening occurs at the point

$$t = \sqrt{\Delta_1 \Delta_2}. \quad (14)$$

In the second setup, there is an additional constraint $\Delta_1 \neq \Delta_2$. If $t > \sqrt{\Delta_1 \Delta_2}$, there is one Kramers pair of MFs localized at the interfaces at $x = 0$ and one at $x = L$ [43]. The localization lengths are inversely proportional to the gaps opened at the Fermi points [44]. Thus, in regions with no tunnel coupling between the TIs the localization lengths are the superconducting coherence lengths $\xi_n = \hbar v_F / \Delta_n$, while in regions with $t > \sqrt{\Delta_1 \Delta_2}$ they are given by

$$\xi^{(1)} = 2\hbar v_F / (\sqrt{(\Delta_1 - \Delta_2)^2 + 4t^2} - \Delta_1 - \Delta_2) \quad (15)$$

$$\xi_{\pm}^{(2)} = \frac{2\hbar v_F}{|\Delta_1 - \Delta_2| \pm \Re \sqrt{(\Delta_1 + \Delta_2)^2 - 4t^2}}. \quad (16)$$

Superscript (1) [(2)] corresponds to first [second] setup and \Re means the real part of a complex number. In both setups we assume that the length of the tunnel barrier L is much longer than the localization lengths $\xi_{\max}^{(1)} \equiv \max\{\xi_1, \xi_2, \xi^{(1)}\}$ ($\xi_{\max}^{(2)} = \max\{\xi_2, \xi^{(2)}\}$ for $\Delta_1 > \Delta_2$ and $\xi_{\max}^{(2)} = \max\{\xi_1, \xi^{(2)}\}$ for $\Delta_1 < \Delta_2$). Hence the wavefunctions of the MFs localized at the two different interfaces do not overlap and can be considered as independent. If L is comparable or shorter than the localization length of the MFs they hybridize into two complex fermionic state whose energies are non-zero in general [45, 46]. Tuning L by underlying gates allows one to arbitrarily control the position of the MFs along the TI edges. To give a numerical estimate of the localization length we assume that the induced gaps are given by $\Delta_1 = 0.1$ meV, $\Delta_2 = 0.2$ meV, and the tunnel coupling is set to $t = 0.2$ meV. In a InAs/GaSb (HgTe/CdTe) TI the Fermi velocity is given by $v_F = 4.6 \times 10^4$ m s⁻¹ [8] (5.5×10^5 m s⁻¹ [11]). This gives a localization length of the order of $0.5 \mu\text{m}$ ($5 \mu\text{m}$). Finally, we emphasize here that the opposite relative sign in front of the proximity induced gaps of the two edges in Eq.(11) is an important ingredient to generate the Kramers pair of MFs. If this relative sign is the same there exists no topological phase. For illustrative phase diagrams, see [44].

Conclusions. We have proposed and studied two setups to realize a proximity-induced $J\pi J$ in a TI in the presence of TRI. Both setups rely on the tunnel coupling of a TI sample to an s -wave bulk SC either via a layer of scalar and magnetic impurities with randomly oriented spins or via an array of QDs each of which is occupied by a randomly oriented spin. We have seen that if in either case spin-flip tunneling dominates over normal tunneling a π -junction emerges. The randomly oriented spins ensure that there is effectively no breaking of TRI. As an application we have demonstrated how such proximity-induced π -junctions can be used to generate and manipulate Kramers pairs of MFs in edge states of tunnel-coupled TIs.

Acknowledgments. We acknowledge support from the Swiss NSF and NCCR QSIT.

-
- [1] L. N. Bulaevskii, V. V. Kuzii, and A. A. Sobyanin, Pis'ma Zh. Eksp. Teor. Fiz. **25**, 314 (1977) [JETP Lett. **25**, 290 (1977)].
- [2] O. Vavra, S. Gazi, D. S. Golubovic, I. Vavra, J. Verbeeck, G. Van Tendeloo, and V. V. Moshchalkov, Phys. Rev. B **74**, 020502(R) (2006).
- [3] A. I. Buzdin and M. Y. Kupriyanov, Pis'ma Zh. Eksp. Teor. Fiz. **52**, 1089 (1990) [JETP Lett. **52**, 487 (1990)].
- [4] V. V. Ryazanov, V. A. Oboznov, A. Yu. Rusanov, A. V. Veretennikov, M. Golubov, and J. Aarts, Phys. Rev. Lett. **86**, 2427 (2001).
- [5] B. I. Spivak and S. A. Kivelson, Phys. Rev. B **43**, 3740 (1991).
- [6] J. A. van Dam, Y. V. Nazarov, E. P. A. M. Bakkers, and L. P. Kouwenhoven, Nature (London) **442**, 667 (2006).
- [7] S. Hart, H. Ren, T. Wagner, P. Leubner, M. Muhlbauer, C. Brune, H. Buhmann, L. Molenkamp, and A. Yacoby, Nature Physics **10**, 638 (2014).
- [8] V. S. Pribiag, A. J. A. Beukman, F. Qu, M. C. Cassidy, C. Charpentier, W. Wegscheider, and L. P. Kouwenhoven, doi:10.1038/nnano.2015.86.
- [9] J. Wiedenmann, E. Bocquillon, R. S. Deacon, S. Hartinger, T. M. Klapwijk, L. Maier, C. Ames, C. Brune, K. Ishibashi, S. Tarucha, H. Buhmann, and L. W. Molenkamp, arXiv:1503.05591.
- [10] M. Z. Hasan and C. L. Kane, Rev. Mod. Phys. **82**, 3045 (2010).
- [11] X.-L. Qi and S.-C. Zhang, Rev. Mod. Phys. **83**, 1057 (2011).
- [12] G. Tkachov and E. M. Hankiewicz, Phys. Status Solidi B **250**, 215 (2013).
- [13] B. A. Volkov and O. A. Pankratov, Pis'ma Zh. Eksp. Teor. Fiz. **42**, 145 (1985) [JETP Lett. **42**, 178 (1985)].
- [14] O. A. Pankratov, S. V. Pakhomov, and B. A. Volkov, Solid State Commun. **61**, 93 (1987).
- [15] B. A. Bernevig, T. L. Hughes, S.-C. Zhang, Science **314**, 1757 (2006).
- [16] M. König, S. Wiedmann, C. Brune, A. Roth, H. Buhmann, L. W. Molenkamp, X.-L. Qi, and S.-C. Zhang, Science **318**, 766 (2007).
- [17] A. Roth, C. Brune, H. Buhmann, L. W. Molenkamp, J. Maciejko, X.-L. Qi, and S.-C. Zhang, Science **325**, 294 (2009).
- [18] K. C. Nowack, E. M. Spanton, M. Baenninger, M. König, J. R. Kirtley, B. Kalisky, C. Ames, P. Leubner, C. Brune, H. Buhmann, L. W. Molenkamp, D. Goldhaber-Gordon, and K. A. Moler, Nature Materials **12**, 787 (2013).
- [19] F. Crepin and B. Trauzettel, Phys. Rev. Lett. **112**, 077002 (2014).
- [20] F. Crepin, B. Trauzettel, and F. Dolcini, Phys. Rev. B **89**, 205115 (2014).
- [21] G. Tkachov, P. Burset, B. Trauzettel, and E. M. Hankiewicz, arXiv:1409.7301v4.
- [22] A. G. Lebed, Pis'ma Zh. Eksp. Teor. Fiz. **43**, 137 (1986) [JETP Lett. **43**, 174 (1986)].
- [23] C. L. Kane, R. Mukhopadhyay, and T. C. Lubensky, Phys. Rev. Lett. **88**, 036401 (2002).
- [24] J. Klinovaja and D. Loss, Phys. Rev. Lett. **111**, 196401 (2013).
- [25] J. C. Y. Teo and C. L. Kane, Phys. Rev. B **89**, 085101 (2014).
- [26] J. Klinovaja and D. Loss, Eur. Phys. J. B **87**, 171 (2014).
- [27] J. Klinovaja and Y. Tserkovnyak, Phys. Rev. B **90**, 115426 (2014).
- [28] J. Klinovaja, Y. Tserkovnyak, and D. Loss, Phys. Rev. B **91**, 085426 (2015).
- [29] C. L. M. Wong and K. T. Law, Phys. Rev. B **86**, 184516 (2012).
- [30] S. Nakosai, J. K. Budich, Y. Tanaka, B. Trauzettel, and N. Nagaosa, Phys. Rev. Lett. **110**, 117002 (2013).
- [31] X.-J. Liu, C. L. M. Wong, and K. T. Law, Phys. Rev. X **4**, 021018 (2014).
- [32] E. Dumitrescu, J. Sau, and S. Tewari, Phys. Rev. B **90**, 245438 (2014).
- [33] F. Zhang, C. L. Kane, and E. J. Mele, Phys. Rev. Lett. **111**, 056402 (2013).
- [34] A. Keselman, L. Fu, A. Stern, and E. Berg, Phys. Rev. Lett. **111**, 116402 (2013).
- [35] A. Haim, A. Keselman, E. Berg, and Y. Oreg, Phys. Rev. B **89**, 220504 (2014).
- [36] E. Gaidamauskas, J. Paaske, and K. Flensberg, Phys. Rev. Lett. **112**, 126402 (2014).
- [37] J. Klinovaja and D. Loss, Phys. Rev. B **90**, 045118 (2014).
- [38] J. Klinovaja, A. Yacoby, and D. Loss, Phys. Rev. B **90**, 155447 (2014).
- [39] C.-X. Liu and B. Trauzettel, Phys. Rev. B **83**, 220510(R) (2011).
- [40] N. Kopnin, Theory of Nonequilibrium Superconductivity, (Oxford University Press, Oxford, 2001).
- [41] J. R. Schrieffer and P. A. Wolff, Phys. Rev. **149**, 491 (1966).
- [42] L. Fu and C. L. Kane, Phys. Rev. Lett. **100**, 096407 (2008).
- [43] J. Klinovaja and D. Loss, Phys. Rev. B **86**, 085408 (2012).
- [44] See Supplemental Material (SM) for more details such as the spectrum, explicit MF wave functions, and plots of phase diagrams with topological and trivial phases.
- [45] D. Rainis, L. Trifunovic, J. Klinovaja, and D. Loss, Phys. Rev. B **87**, 024515 (2013).
- [46] A. A. Zyuzin, D. Rainis, J. Klinovaja, and D. Loss, Phys. Rev. Lett. **111**, 056802 (2013).

Supplemental Material to ‘Proximity-induced Josephson π -junctions in topological insulators’

Constantin Schrader, A.A. Zyuzin, Jelena Klinovaja, and Daniel Loss

Department of Physics, University of Basel, Klingelbergstrasse 82, CH-4056 Basel, Switzerland

In the Supplemental Material, we derive the MF wavefunctions for two models introduced in the main text.

Energy spectrum

We find that the bulk spectrum of the Hamiltonian $H^{(1)}$ from the main text is given by

$$E_{1,s,\pm}(k) = s \left[(\hbar v_F k)^2 + \left(\Delta_+ \pm \sqrt{\Delta_-^2 + t^2} \right)^2 \right]^{1/2}, \quad (\text{S1})$$

where k is the momentum in the TI, and $s = \pm 1$. Similarly the bulk spectrum of the Hamiltonian $H^{(2)}$ from the main text is given by

$$E_{2,s,\pm}(k) = s \left[(\hbar v_F k)^2 + \Delta_+^2 + \Delta_-^2 + t^2 \pm 2\sqrt{W(k)} \right]^{1/2} \quad (\text{S2})$$

with $W(k) = (\hbar v_F k)^2 t^2 + \Delta_+^2 (\Delta_-^2 + t^2)$. Here, we also introduced the notations $\Delta_{\pm} = (\Delta_1 \pm \Delta_2)/2$. Both spectra $E_{1,s,\pm}(k)$ and $E_{2,s,\pm}(k)$ are twofold degenerate as expected for time-reversal invariant systems.

We find that the spectrum is gapless at $k = 0$ if

$$t = \sqrt{\Delta_1 \Delta_2}, \quad (\text{S3})$$

and is gapped otherwise. Here, for setup $N = 2$ we need the additional condition that $\Delta_1 \neq \Delta_2$. Also the spectral gap for the setup $N = 2$ closes at some finite momentum

if $t > \Delta_1 = \Delta_2$. We now assume that $\Delta_1 \neq \Delta_2$ and confirm that Eq. (S3) defines a topological phase transition. This means that there should be MFs localized at the boundary between two space regions with $t > \sqrt{\Delta_1 \Delta_2}$ and $t < \sqrt{\Delta_1 \Delta_2}$.

Wavefunctions and localization lengths of MFs

The operator defining a MF, which is a zero-energy bound state, is generally given by $\gamma_j^{(N)} \equiv (\gamma_j^{(N)})^\dagger = \sum_{n=1,2} \int dx \psi_{n,j}^{(N)}(x) \cdot \Phi_n(x)$ with the wavefunction (vector)

$$(\psi_{n,j}^{(N)})^T(x) = \begin{pmatrix} f_{n,j}^{(N)}(x) \\ g_{n,j}^{(N)}(x) \\ (f_{n,j}^{(N)})^*(x) \\ (g_{n,j}^{(N)})^*(x) \end{pmatrix} \quad (\text{S4})$$

for some complex-valued functions $f_{n,j}^{(N)}(x)$ and $g_{n,j}^{(N)}(x)$. The index $j = 1, 2$ distinguishes between two MFs belonging to the same Kramers pair. The form of these functions is different for different setups.

Without loss of generality, we focus below on the left interfaces at which the tunneling amplitude jumps from $t = 0$ at $x < 0$ to $t = t_0 > \sqrt{\Delta_1 \Delta_2}$ for $x > 0$.

First setup. We find that for the first setup the interface hosts a Kramers pair of MFs given by

$$-i f_{n,1}^{(1)} = (g_{n,1}^{(1)})^* = \begin{cases} \left(\delta_{n1} \frac{\sqrt{\Delta_-^2 + t_0^2} - \Delta_-}{t_0} e^{ik_F x} + \delta_{n2} e^{-ik_F x} \right) e^{\frac{i\phi}{2}} e^{-x/\xi^{(1)}} & \text{if } x > 0 \\ \left(\delta_{n1} \frac{\sqrt{\Delta_-^2 + t_0^2} - \Delta_-}{t_0} e^{ik_F x} e^{x/\xi_1} + \delta_{n2} e^{-ik_F x} e^{x/\xi_2} \right) e^{\frac{i\phi}{2}} & \text{if } x < 0 \end{cases}, \quad (\text{S5})$$

$$f_{n,2}^{(1)} = (-1)^n (g_{n,1}^{(1)})^*, \quad g_{n,2}^{(1)} = (-1)^{n-1} (f_{n,1}^{(1)})^*$$

with the localization lengths given by

$$\xi^{(1)} = \hbar v_F / (\sqrt{\Delta_-^2 + t_0^2} - \Delta_+) \quad (\text{S6})$$

$$\xi_n = \hbar v_F / \Delta_n.$$

In Fig. S1(a) the localization length $\xi^{(1)}$ is plotted for different values of t_0 in color scale versus Δ_1 and

Δ_2 . Note that the solutions for given N are orthogonal, $\psi_{n,1}^{(N)} \cdot (\psi_{n,2}^{(N)})^T = 0$, thus forming a Kramers pair. The localization length of the MF is given by $\xi_{\max}^{(1)} = \max\{\xi^{(1)}, \xi_1, \xi_2\}$ and is plotted in Fig. S1(b).

Second setup. The interface at $x = 0$ of the second setup also hosts a Kramers pair of MFs. For $\Delta_- > 0$ the Kramers pair of MFs is given by

$$f_{n,1}^{(2)} = e^{ik_F x} \begin{cases} i\delta_{n2} \left(\frac{\Delta_+ - \sqrt{\Delta_+^2 - t_0^2}}{2\sqrt{\Delta_+^2 - t_0^2}} e^{-x/\xi_+^{(2)}} - \frac{\Delta_+ + \sqrt{\Delta_+^2 - t_0^2}}{2\sqrt{\Delta_+^2 - t_0^2}} e^{-x/\xi_-^{(2)}} \right) e^{i\frac{\phi}{2}} - \frac{\delta_{n1}(e^{-x/\xi_-^{(2)}} - e^{-x/\xi_+^{(2)}})t_0 e^{-i\frac{\phi}{2}}}{2\sqrt{\Delta_+^2 - t_0^2}} & \text{if } x \geq 0, \Delta_+ > t_0 \\ - \left(\delta_{n1} \frac{t_0 x}{\hbar v_F} e^{-i\frac{\phi}{2}} + i\delta_{n2} \left(1 + \frac{t_0 x}{\hbar v_F} \right) e^{i\frac{\phi}{2}} \right) e^{-x/\xi_{\pm}^{(2)}} & \text{if } x \geq 0, \Delta_+ = t_0 \\ - \left(\delta_{n1} \frac{t_0 \sin(k^{(2)}x)}{\sqrt{t_0^2 - \Delta_+^2}} e^{-i\frac{\phi}{2}} + i\delta_{n2} \left(\frac{\Delta_+ \sin(k^{(2)}x)}{\sqrt{t_0^2 - \Delta_+^2}} + \cos(k^{(2)}x) \right) e^{i\frac{\phi}{2}} \right) e^{-x/\xi_{\pm}^{(2)}} & \text{if } x \geq 0, \Delta_+ < t_0 \\ -i\delta_{n2} e^{i\frac{\phi}{2}} e^{x/\xi_2} & \text{if } x < 0 \end{cases},$$

$$g_{n,1}^{(2)} = i(f_{n,1}^{(2)})^*, \quad f_{n,2}^{(2)} = -(g_{n,1}^{(2)})^*, \quad g_{n,2}^{(2)} = (f_{n,1}^{(2)})^*,$$
(S7)

while for $\Delta_- < 0$ it is given by

$$f_{n,1}^{(2)} = e^{ik_F x} \begin{cases} \frac{i\delta_{n2} \left(e^{-x/\xi_+^{(2)}} - e^{-x/\xi_-^{(2)}} \right) t_0 e^{i\frac{\phi}{2}}}{2\sqrt{\Delta_+^2 - t_0^2}} - \delta_{n1} \left(\frac{\Delta_+ - \sqrt{\Delta_+^2 - t_0^2}}{2\sqrt{\Delta_+^2 - t_0^2}} e^{-x/\xi_+^{(2)}} - \frac{\Delta_+ + \sqrt{\Delta_+^2 - t_0^2}}{2\sqrt{\Delta_+^2 - t_0^2}} e^{-x/\xi_-^{(2)}} \right) e^{-i\frac{\phi}{2}} & \text{if } x \geq 0, \Delta_+ > t_0 \\ \left(\delta_{n1} \left(1 + \frac{t_0 x}{\hbar v_F} \right) e^{-i\frac{\phi}{2}} - i\delta_{n2} \frac{t_0 x}{\hbar v_F} e^{i\frac{\phi}{2}} \right) e^{-x/\xi_{\pm}^{(2)}} & \text{if } x \geq 0, \Delta_+ = t_0 \\ \left(\delta_{n1} \left(\frac{\Delta_+ \sin(k^{(2)}x)}{\sqrt{t_0^2 - \Delta_+^2}} + \cos(k^{(2)}x) \right) e^{-i\frac{\phi}{2}} - i\delta_{n2} \frac{t_0 \sin(k^{(2)}x)}{\sqrt{t_0^2 - \Delta_+^2}} e^{i\frac{\phi}{2}} \right) e^{-x/\xi_{\pm}^{(2)}} & \text{if } x \geq 0, \Delta_+ < t_0 \\ \delta_{n1} e^{-i\frac{\phi}{2}} e^{x/\xi_1} & \text{if } x < 0 \end{cases},$$

$$g_{n,1}^{(2)} = i(f_{n,1}^{(2)})^*, \quad f_{n,2}^{(2)} = -(g_{n,1}^{(2)})^*, \quad g_{n,2}^{(2)} = (f_{n,1}^{(2)})^*.$$
(S8)

Again, the two wavefunctions for given N are orthogonal and thus forming a Kramers pair. We have defined the wavenumber

$$k^{(2)} = \sqrt{|\Delta_+^2 - t_0^2|}/\hbar v_F \quad (\text{S9})$$

and the localization lengths

$$\xi_{\pm}^{(2)} = \frac{\hbar v_F}{|\Delta_-| \pm \Re \sqrt{\Delta_+^2 - t_0^2}}. \quad (\text{S10})$$

For different values of t_0 the localization lengths $\xi_{\pm}^{(2)}$ are displayed in Fig. S1(c) and (d) in a color scale plot as a function of Δ_1 and Δ_2 . For $t_0 \leq \Delta_+$ the spectral gap closes at zero momentum while for $t_0 > \Delta_+$ it closes at some finite momentum. For $\Delta_- > 0$ ($\Delta_- < 0$) the localization length of the MF is given by $\xi_{\max}^{(2)} = \max\{\xi_2, \xi_-^{(2)}\}$

($\xi_{\max}^{(2)} = \max\{\xi_1, \xi_-^{(2)}\}$) and is plotted in Fig. S1(e). The fast-oscillating factors have explicitly been restored in the wavefunctions. We see that for $\Delta_1 = \Delta_2$ the MF wavefunction is delocalized. In the limit when $L \gg \xi_{\max}^{(N)}$ the interfaces at $x = 0$ and $x = L$ can be considered as independent and a calculation of the MF wavefunctions at $x = L$ can be performed analogously.

Finally for setup N the tunneling phase ϕ can be absorbed into a redefinition of the electron operators by the gauge transformations

$$\begin{aligned} R_n &\mapsto \exp \left((-1)^{n(N-1)} \frac{i\phi}{2} \right) R_n \\ L_n &\mapsto \exp \left(-(-1)^{n(N-1)} \frac{i\phi}{2} \right) L_n. \end{aligned} \quad (\text{S11})$$

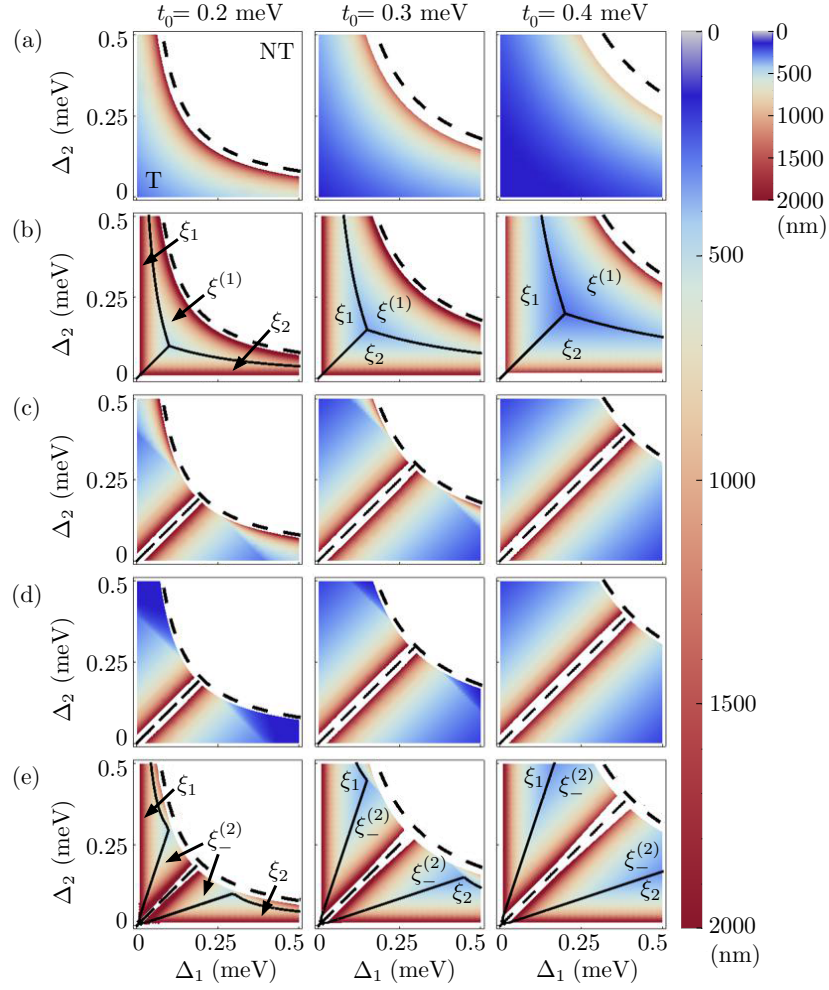


Figure S1: (Color online) (a) Phase diagrams and color scale plots of the localization length $\xi^{(1)}$ for $x > 0$ of the Kramers pair of MFs in the first setup as a function of the superconducting gap parameters $\Delta_{1,2}$ and the tunneling amplitude t_0 . Here, $\xi^{(1)}$ increases from blue, through yellow, to red; $v_F = 4.6 \times 10^4 \text{ ms}^{-1}$ in an InAs/GaSb TI [8]. The curve $t_0 = \sqrt{\Delta_1 \Delta_2}$ (dashed) separates the topological phase (T, colored) and the non-topological phase (NT, uncolored). At the phase boundary the localization length $\xi^{(1)}$ is divergent. For $x < 0$ the localization lengths are given by the superconducting coherence lengths $\xi_{1,2} = \hbar v_F / \Delta_{1,2}$. (b) Same as in (a) but for $\xi_{\max}^{(1)} \equiv \max\{\xi_1, \xi_2, \xi^{(1)}\}$. The curves $\xi_{1,2} = \xi^{(1)}$ and $\xi_1 = \xi_2$ (solid) separate regions where $\xi_{\max}^{(1)}$ is given respectively by ξ_1, ξ_2 or $\xi^{(1)}$. (c) Same as in (a) but for the localization length $\xi_{\pm}^{(2)}$ for $x > 0$ in the second setup. Along the line $\Delta_1 = \Delta_2$ (dashed) the localization lengths $\xi_{\pm}^{(2)}$ are divergent. (d) Same as in (c) but for the localization length $\xi_+^{(2)}$. (e) Same as in (d) but for $\xi_{\max}^{(2)} = \max\{\xi_2, \xi_{-}^{(2)}\}$ if $\Delta_1 > \Delta_2$ and $\xi_{\max}^{(2)} = \max\{\xi_1, \xi_{-}^{(2)}\}$ if $\Delta_1 < \Delta_2$. The curves $\xi_{1,2} = \xi_{-}^{(2)}$ (solid) separate regions where $\xi_{\max}^{(2)}$ is given respectively by ξ_1, ξ_2 or $\xi_{-}^{(2)}$.